



Review

Interplay between conformational selection and induced fit in multidomain protein–ligand binding probed by paramagnetic relaxation enhancement



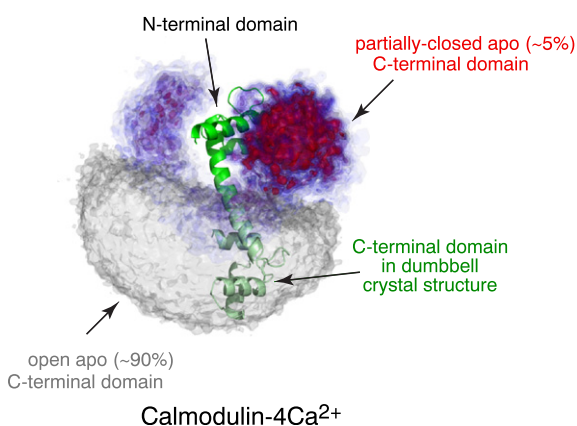
G. Marius Clore*

Laboratory of Chemical Physics, National Institute of Diabetes and Digestive and Kidney Diseases, National Institutes of Health, Bethesda, MD 20892-0520, USA

HIGHLIGHTS

- Sparsely-populated species can be detected by paramagnetic relaxation enhancement.
- Maltose-binding protein and calmodulin exist as a mixture of open and partially-closed states in the absence of bound ligand.
- The partially-closed states occupy a region of conformational space in the vicinity of the holo state.
- Partially closed-states may facilitate the transition to the holo state upon ligand binding.

GRAPHICAL ABSTRACT



ARTICLE INFO

Article history:

Received 2 August 2013
 Received in revised form 24 August 2013
 Accepted 24 August 2013
 Available online 31 August 2013

Keywords:

Paramagnetic relaxation enhancement
 Sparsely-populated transient state
 Conformational selection
 Induced fit
 Maltose binding protein
 Calmodulin

ABSTRACT

The binding of ligands and substrates to proteins has been extensively studied for many years and can be described, in its simplest form, by two limiting mechanisms: conformational selection and induced fit. Conformational selection involves the binding of ligand to a pre-existing sparsely-populated conformation of the free protein that is the same as that in the final protein–ligand complex. In the case of induced fit, the ligand binds to the major conformation of the free protein and only subsequent to binding undergoes a conformational change to the final protein–ligand complex. While these two mechanisms can be dissected and distinguished by transient kinetic measurements, direct direction, characterization and visualization of transient, sparsely-populated states of proteins are experimentally challenging. Unless trapped, sparsely-populated states are generally invisible to conventional structural and biophysical techniques, including crystallography and most NMR measurements. In this review we summarize some recent developments in the use of paramagnetic relaxation enhancement to directly study sparsely-populated states of proteins and illustrate the application of this approach to two proteins, maltose binding protein and calmodulin, both of which undergo large rigid body conformational rearrangements upon ligand binding from an open apo state to a closed ligand-bound holo state. We show that the apo state ensemble comprises a small population of partially-closed configurations that are similar but not identical to that of the holo state. These results highlight the complementarity and interplay of induced fit and conformational selection and suggest that the existence of partially-closed states in the absence of ligand facilitates the transition to the closed ligand-bound state.

Published by Elsevier B.V.

* Tel.: +1 301 496 0782; fax: +1 301 496 0825.
 E-mail address: mariusc@mail.nih.gov.

Contents

1. Introduction	4
2. Underlying basis for detecting sparsely-populated states by PRE	4
3. Maltose binding protein	5
4. Calmodulin	10
5. Concluding remarks	11
Acknowledgments	11
References	11

1. Introduction

Protein interactions are crucial to all aspects of cell function. In its simplest form, the interaction of a protein with a ligand (which may be a small molecular weight substrate, another protein, or an intrinsically disordered peptide) can be described by two limiting mechanisms [1–10]: conformational selection or induced fit (Fig. 1). In the case of conformational selection, the protein exists in a dynamic equilibrium between major and minor species, and the substrate selectively binds the minor species leading to the formation of the protein–ligand complex. In the case of induced fit, the ligand binds to the major species followed by a conformational change in the initial (weak) complex that results in the formation of the final protein–ligand complex. These two mechanisms, which have been the subject of extensive investigation for the last 50 years, can potentially be distinguished by transient kinetic measurements, and the relative importance of conformational selection and induced fit for a given protein–ligand interaction can be assessed by comparing the fluxes through each pathway [8]. In reality, the choice of which pathway is actually followed is not an all or nothing phenomenon. Rather, in many instances both mechanisms may be operational and the preferred reaction path can be modulated by the protein and ligand concentrations.

Experimental characterization of sparsely-populated states of proteins that may be involved in conformational selection, is technically challenging, since in general such short-lived states are invisible to structural and biophysical techniques, including crystallography and conventional NMR spectroscopy [11,12]. In this brief review we summarize some recent developments in NMR involving paramagnetic relaxation enhancement (PRE) that permits such sparsely-populated states to be directly detected and in suitable cases visualized, and illustrate the application of this methodology to two proteins,

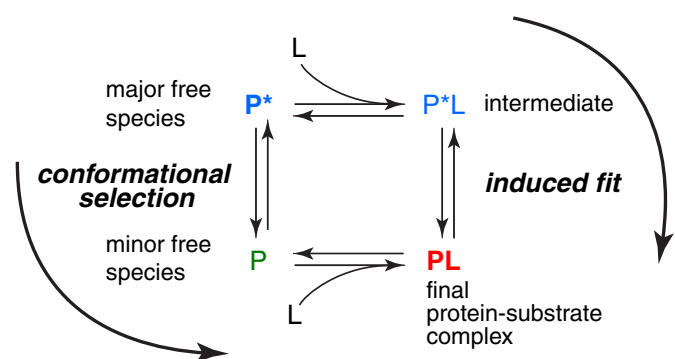


Fig. 1. Simple scheme for conformational selection and induced fit. The protein exists in two states, a major species P^* and a minor species P . In the case of conformational selection, the ligand L binds to the minor species P resulting in the formation of the specific complex PL , in which the conformation of the protein is the same as that of the free minor species P . In the case of induced fit, binding of the ligand to the major species P^* results in the formation of an intermediate P^*L in which the protein conformation is the same as that in the free P^* ; a subsequent conformational change results in the formation of the final complex PL .

maltose binding protein (MBP) [13] and calmodulin (CaM) [14], where ligand binding involves large scale rigid-body interdomain rearrangements. In both instances the bound ligand in the holo state is effectively buried from solvent. Consequently, if an unliganded closed state with the same interdomain configuration as that observed in the ligand-bound holo state existed in free solution, the ligand binding site would be occluded and unavailable to bind ligand. Thus, in both instances ligand binding most likely involves a more subtle interplay between conformational selection and induced fit than that envisioned by the simple scheme shown in Fig. 1.

2. Underlying basis for detecting sparsely-populated states by PRE

PRE measurements generally involve covalent linkage of a paramagnetic label such as EDTA- Mn^{2+} or nitroxide to the protein of interest via an engineered surface exposed cysteine residue [15]. The magnitude of the PRE is directly proportional to the $\langle r^{-6} \rangle$ average of the separation between the paramagnetic center and protons of interest. Although the distance dependence of the PRE is the same as that of the interproton nuclear Overhauser effect (NOE) which provides the main source of geometric information used in NMR structure calculations [16], the PRE is much larger than the NOE owing to the large magnetic moment of an unpaired electron [15]. As a result the PRE is detectable up to distances of 25–35 Å depending on the nature of the paramagnetic label, compared to only 5–6 Å for the 1H - 1H NOE.

The transverse PRE rate, Γ_2 , is measured by taking the difference in transverse relaxation rates measured on a paramagnetic sample and a diamagnetic control (e.g. a paramagnetic EDTA- Mn^{2+} tag versus a diamagnetic EDTA- Ca^{2+} tag) [17]. In a system where two or more species are in fast exchange on the PRE time scale (i.e. the overall exchange rate constant k_{ex} for interconversion between the species is much larger than the difference in Γ_2 rates for a particular paramagnetic center–proton interaction), the value of the observed PRE rate, Γ_2^{obs} , is simply given by the population weighted average of the PRE rates for the component species [11,15]. Under these conditions, the footprint of the spectroscopically invisible minor species can be observed on the PRE profiles measured on the NMR resonances of the major species providing there are paramagnetic center–proton distances that are shorter in the former than the latter [11,12]. Sparsely-populated states with paramagnetic center–proton distances that are longer than in the major species will not contribute to the observed PRE profiles.

As an example consider a system comprising a major species at an occupancy (p_{major}) of 99% and a minor species at a population of 1% with a paramagnetic center–proton distance of 30 and 8 Å, respectively [11]. For a 20–30 kDa system paramagnetically tagged with Mn^{2+} , the corresponding Γ_2 rates will be ~ 2 and ~ 5600 s^{-1} , respectively. The dependence of Γ_2^{obs} on k_{ex} can be calculated numerically by solving the McConnell equations. When exchange is fast ($k_{ex} \sim 4 \times 10^4$ s^{-1}), $\Gamma_2^{obs} = 51$ $s^{-1} \sim p_{major}\Gamma_2^{major} + (1-p_{major})\Gamma_2^{minor}$; when exchange is slow ($k_{ex} = 40$ s^{-1}), $\Gamma_2^{obs} = \Gamma_2^{major} = 2$ s^{-1} ; when exchange is intermediate ($k_{ex} = 4000$ s^{-1}), Γ_2^{obs} is calculated to be 25 s^{-1} . Thus, even

in the case of intermediate exchange the footprint of the minor species will be apparent in the PRE profile for the major species. Moreover, because of the $\langle r^{-6} \rangle$ dependence of the PRE, the intermediate exchange example would only result in a 13% overestimation in the value of r_{minor} (9 versus 8 Å) calculated on the fast exchange assumption that Γ_2^{obs} is a population weighted average of the Γ_2 values in the two states.

3. Maltose binding protein

Maltose binding protein (MBP) is a member of the bacterial periplasmic binding protein family that has generally been described to function as “Venus-fly trap” [18]. MBP comprises two domains, an N-terminal domain (NTD) and a C-terminal domain (CTD), whose relative orientation differs by about $\sim 35^\circ$ between the open apo and closed holo states (Fig. 2A) [19,20]. The transition between the two states involves hinge bending within the linker region comprising relatively few residues. Solution residual dipolar couplings (RDCs) measured on apo and holo (maltotriose-bound) MBP in weakly-

aligning media indicate unambiguously that the structures of these two states in solution are the same as those of the corresponding apo and holo crystal structures [21]. However, the observed RDCs are linear population-weighted averages of the species present in solution, and the presence of a small amount of holo state in the absence of ligand would not significantly impact the agreement between the RDCs measured on the apo state and the crystal structure of the apo state [13]. The same is also true of small angle X-ray scattering [13]. The question therefore arises as to whether the apo state exists as a single species in which the closed holo conformation is inaccessible in the absence of ligand and interdomain rearrangement only occurs subsequent to the formation of an initial complex with the apo state (i.e. induced fit), or whether the major open state exists in rapid equilibrium with a sparsely-populated partially-closed state that is still accessible to ligand but is structurally reasonably close to the holo closed state. In the latter instance, ligand could bind to the partially-closed state (conformational selection), followed by a final conformational rearrangement to the closed state (induced fit).

PRE profiles for apo and holo (maltotriose-bound) MBP resulting from the introduction of a nitroxide spin label on the NTD at position

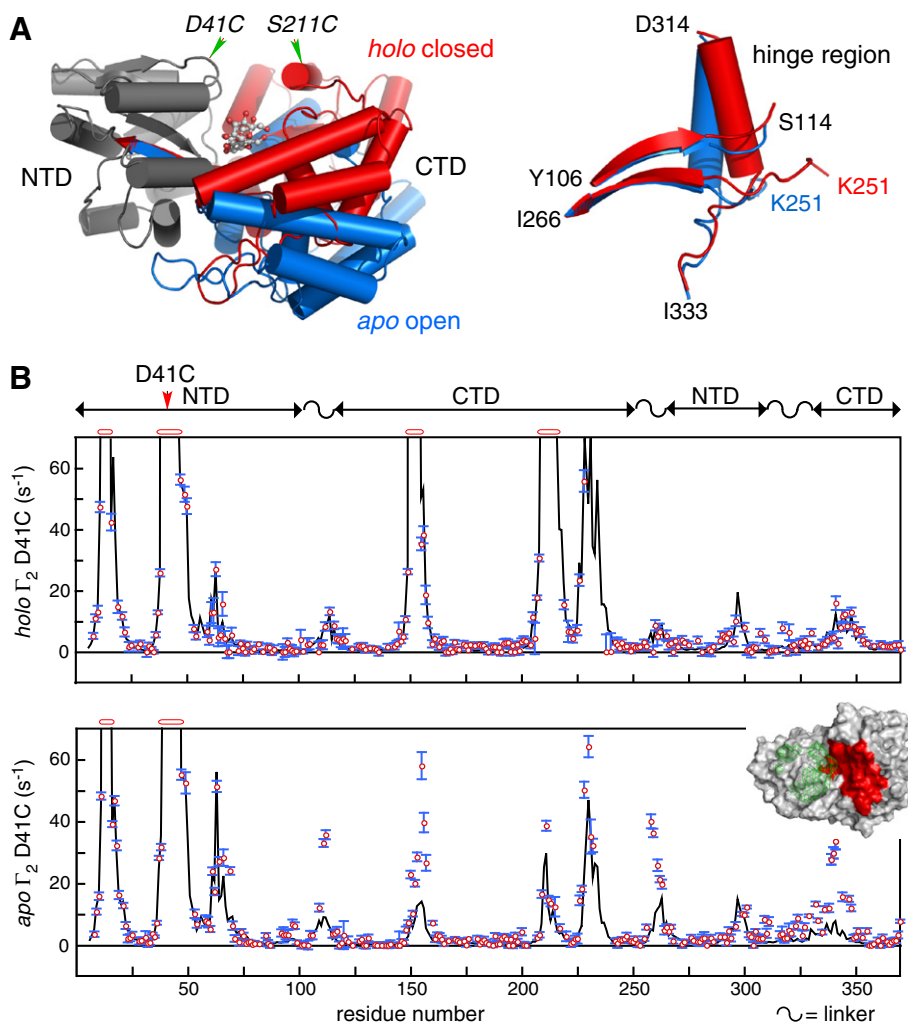


Fig. 2. PRE data provide direct evidence that free MBP exists as a dynamic equilibrium mixture of major and minor species. (A) Comparison of the crystal structures of MBP in the apo open (1OMP [19]) and holo (maltotriose-bound) closed (3MBP [20]) conformations illustrating domain rearrangement upon ligand binding. The left panel shows the two structures with the NTDs (gray) superimposed, and the CTDs in the apo and holo states shown in blue and red, respectively. The location of the two nitroxide spin labels attached (one per sample) to D41C in the NTD and S211C in the CTD is indicated. The right panel shows a close-up of the linker region. (B) Comparison of experimental PRE profiles (red circles) for holo (maltotriose-bound) (top) and apo (bottom) MBP spin-labeled at position D41C in the NTD with the PRE profiles back-calculated from the crystal structure of apo and holo MBP (black lines) [13]. In both cases there is good agreement between observed and calculated values for the intradomain PREs; while good agreement is also obtained for the interdomain PREs in the case of holo MBP, large deviations in the magnitude of the experimental and back-calculated interdomain PREs are observed for apo MBP. This discrepancy cannot be accounted for by a simple linear combination of apo and holo PREs. Adapted from [13].

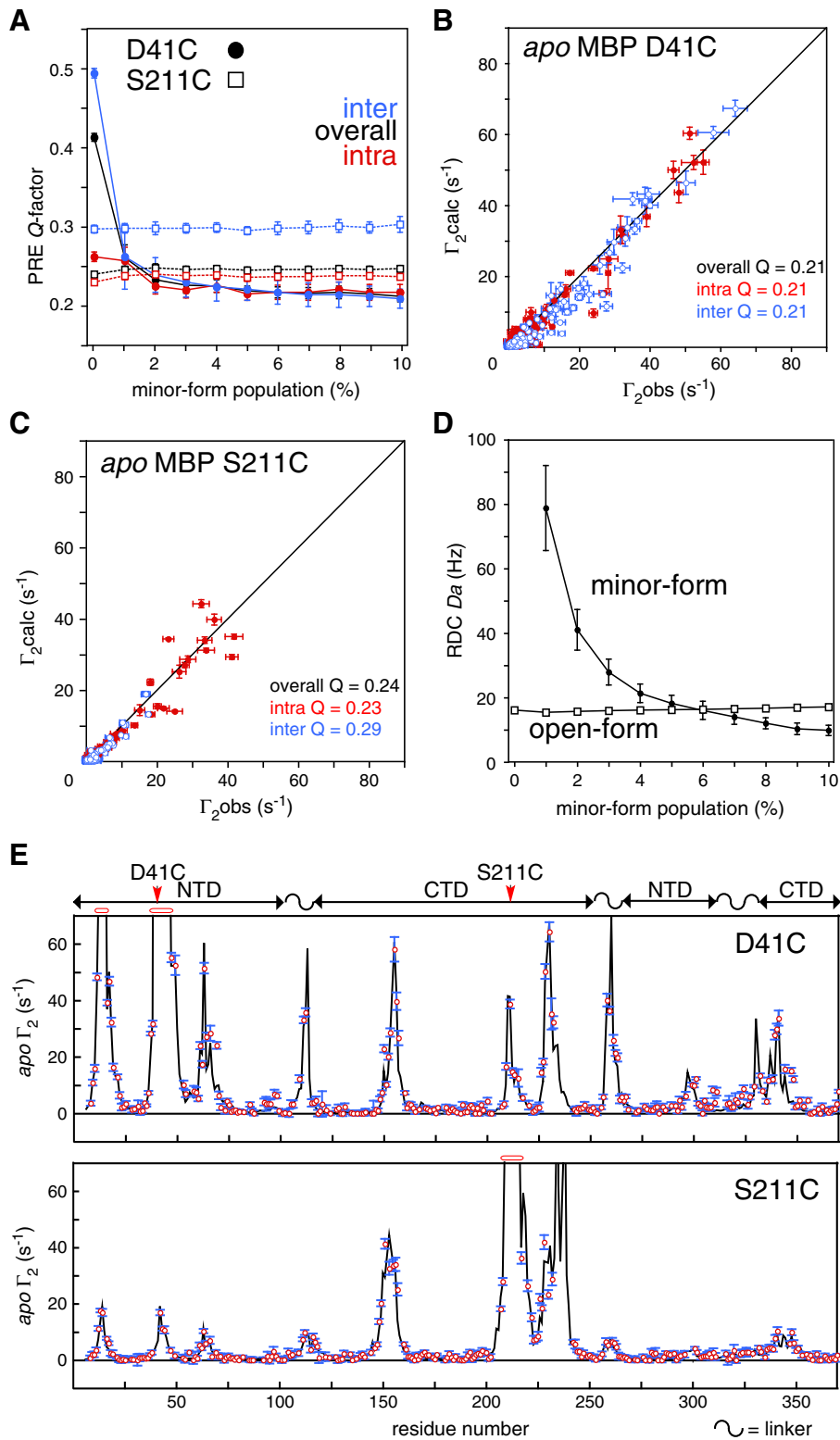


Fig. 3. PRE-driven conjoint rigid body/torsion angle simulated annealing refinement of the minor species of apo MBP [13]. The calculated PREs are represented by a population-weighted average of the PREs for the apo open state (whose structure is known from crystallography) and a partially-closed state. (A) PRE Q-factor as a function of the population of the minor species with filled-in and open symbols representing the results obtained with the nitroxide label at positions D41C and S211C, respectively. Agreement between observed and calculated PREs arising from the spin label at positions (B) D41C and (C) S211C at a population of 5% for the minor species. (D) Magnitude of the principal component (D_a) of the alignment tensors for the major (open-squares) and minor (filled-in circles) species obtained by singular value decomposition. Since the shape and charge distribution of the major and minor species of apo MBP, are very similar the values of D_a for the major and minor species are expected to be similar, allowing the population of the minor species to be estimated more accurately than from the PRE data alone. (E) Comparison of observed (red circles) and calculated (black lines) PRE profiles originating from the spin-label attached to D41C (top) and S211C (bottom) for a 5% population of the minor species. Adapted from [13].

D41C are shown in Fig. 2B [13]. In both instances, the intradomain PREs are in excellent agreement with the values calculated from the two respective crystal structures. However, while the interdomain PREs in the case of holo MBP are in good agreement with the corresponding crystal structure, those for apo MBP reveal significant discrepancies. Specifically, while the peaks in the observed and calculated interdomain PRE profiles for apo MBP are located at the same positions, the calculated interdomain PREs are much smaller than the observed ones. Moreover, the observed PRE profile for apo MBP cannot be reproduced by a linear combination of calculated PREs from the apo and holo crystal structures [13]. The reason that the interdomain PRE profiles for the ligand-bound holo species agree with the crystal structure of the holo state and do not reveal the presence of any sparsely-populated open, partially-open or partially-closed states is due to the fact that if such states exist and are populated at

the 1–5% level (or higher), the interdomain paramagnetic center–proton distances in these states are longer than in the holo state, and therefore will not contribute to the observed PRE (see Section 2).

The simplest interpretation of the PRE data for apo MBP is that the orientation of the NTD and CTD domains in solution is different from that in the crystal structure. Indeed a single structure can be found by rigid-body refinement that satisfies the PRE data. But such an interpretation would in fact be incorrect as the single structure that can satisfy the PRE data is inconsistent with the RDC data (the RDC R-factor increases from 14% to $24 \pm 3\%$) [13]. This leads one to the conclusion that unliganded MBP exists in at least two states in solution, one corresponding to the open apo state seen in the unliganded crystal structure and one or more sparsely-populated states.

The nature of the sparsely-populated state of unliganded MBP can be determined by PRE-driven conjoined rigid body/torsion angle simulated

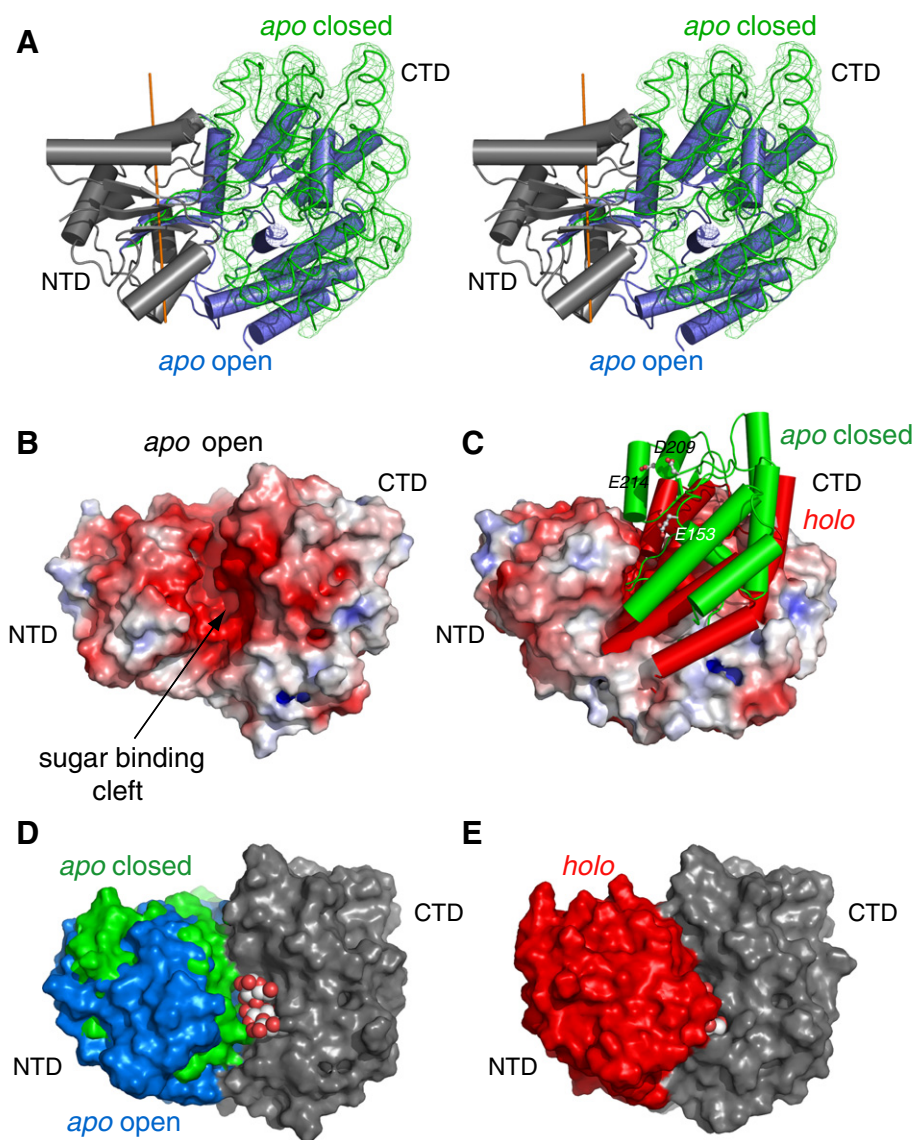


Fig. 4. Structure of the partially-closed apo state of MBP (2V93 [13]). (A) Stereoview showing a superposition of the major open (blue cylinders) and minor partially-closed (green tubes) states of apo MBP with the NTDs (gray) of the two species superimposed. The reweighted atomic probability map [42] for the backbone heavy atoms of the CTD in the partially-closed state is displayed as a green mesh plotted at a threshold of 20%. (B) Electrostatic potential surface of the open form of apo MBP (1OMP [19]) illustrating the high density of negative charge in the sugar binding pocket. (C) Structural comparison of the CTD in the partially-closed form of apo MBP (green cylinders; 2 V93 [13]) and holo MBP (red cylinders; 3MBP [20]) with the apo open state shown as a molecular surface color coded according to electrostatic potential. (D) Molecular surface representation of the major open and minor partially-closed states of apo MBP best-fitted to the CTD (gray) with the NTD displayed in blue and green, respectively. A space-filling representation of maltotriose is modeled bound to the CTD. (E) Holo MBP in the same view as in (D) with the NTD shown in red and the CTD in gray; the substrate is buried in holo MBP and is barely visible. Adapted from [13].

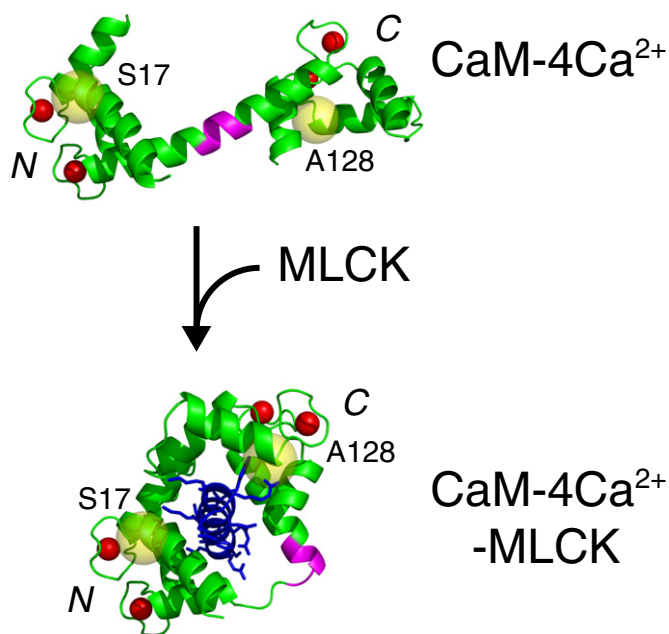


Fig. 5. Comparison of the crystal structure of CaM-4Ca²⁺ (1CLL [35]; top) in the extended dumbbell conformation with a contiguous central helix and the crystal structure of the CaM-4Ca²⁺/MLCK peptide complex (1CDL [32]; bottom). The Ca²⁺ ions and the spin-labeling sites in the NTD (S17C) and CTD (A128C) are shown as red and yellow spheres, respectively; the flexible linker (residues 77–81) in magenta; and the bound MLCK peptide in blue.

Adapted from [14].

annealing [22–24] in which the NTD and CTD are treated as rigid bodies and the linker regions are given torsional degrees of freedom [13]. The overall calculated PRE is given by the population-weighted average of the calculated PREs for the open apo state (whose known structure is held fixed) and the sparsely-populated state. These calculations (Fig. 3) yield excellent agreement with the experimental PRE data using a single minor state with a population of ~5% (as assessed from the RDC data; at a population of 5% of the minor species, the magnitude of the principal component of the calculated alignment tensors of the major and minor species are comparable [13]). The overall backbone precision for the minor species coordinates is 1.3 ± 0.4 Å, and the

backbone precision for the CTD when best-fitting to the NTD is 3.1 ± 1.0 Å, with an uncertainty in the relative orientation of the two domains of $10 \pm 4^\circ$ (Fig. 4A). Additional calculations in which the minor state is represented by an ensemble rather than a single structure yield very similar results: the conformational space sampled by the ensemble, while somewhat larger, overlaps with that sampled by the single structure representation and the mean coordinate positions for the single structure and ensemble representations are very close to one another.

The sparsely-populated species of apo MBP is a partially-closed state characterized by a $\sim 33^\circ$ hinge rotation relative to the open apo state [13] (Fig. 4A). The partially-closed apo state and the closed holo state differ from one another by an $\sim 18^\circ$ reorientation of the domains and a 6 Å translation [13] (Fig. 4C). While the sugar binding sites on the NTD and CTD are fully accessible in the apo open state and completely occluded in the closed holo state, the NTD sugar-binding site is partially occluded and the CTD sugar-binding site exposed in the partially-closed apo state. The interface between the NTD and CTD is lined by negatively charged residues (Fig. 4B) that are responsible for a large array of hydrogen bonds (both direct and water bridged) with the sugar in the closed holo state (Fig. 4E). However, when the sugar is removed, the energy landscape is altered and access to the closed holo structure is energetically highly unfavorable owing to electrostatic repulsion and lack of interdomain complementarity within the ligand-binding cleft that cannot be offset by bridging water molecules. Indeed, the occupancy of a closed holo state in the absence of ligand has been calculated at less than 0.001% based on combined analysis of mutational, fluorescence and NMR data that systematically examined the energetic cost of domain reorientation [25]. Unfavorable interdomain electrostatic repulsion in the apo partially-closed state is avoided by the ~ 6 Å translation of the CTD relative to its position in the closed state, which increases the interdomain separation between negatively charged residues lining the sugar binding cleft (Fig. 4C) and leaves the sugar binding surface on the CTD accessible to an incoming sugar molecule (Fig. 4D).

The PRE data demonstrate unambiguously the existence of a dynamic equilibrium between open and partially-closed apo states of MBP. The lower and upper limits of the exchange time scale between these two states can be estimated to be 20 ns (from heteronuclear ¹⁵N-¹H NOE data) and 20 μs (from relaxation dispersion), respectively [13]. Since the PREs are measured at equilibrium, the NMR data do not provide any information regarding the pathway of ligand binding. One can surmise, however, that the

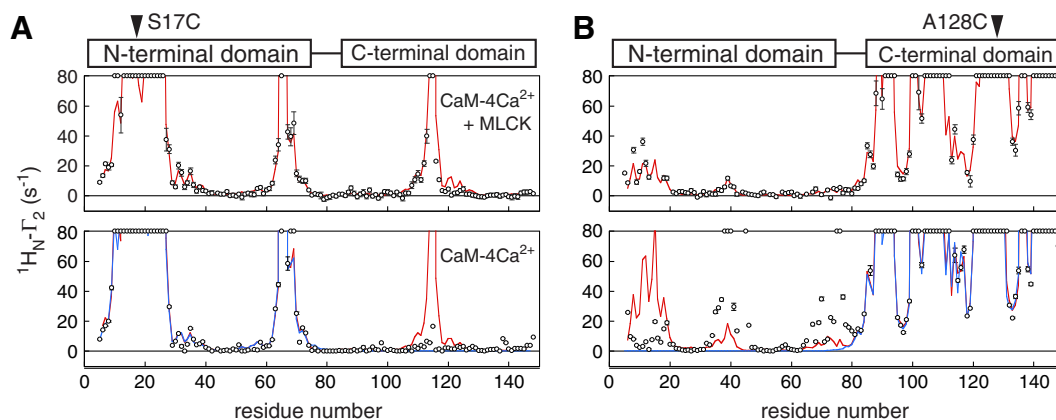


Fig. 6. Comparison of PRE profiles observed for the CaM-4Ca²⁺/MLCK complex (top) and free CaM-4Ca²⁺ (bottom) with the spin-label located in either the NTD (A) or CTD (B). The experimental PRE profiles are shown as open circles, and PREs back-calculated from the crystal structures of CaM-4Ca²⁺/MLCK [32] and CaM-4Ca²⁺ [35] are displayed as red and blue lines respectively. The intra- and interdomain PREs are well-predicted for the peptide-bound state. For CaM-4Ca²⁺, however, only the intradomain PREs are well-predicted, and the observed interdomain PREs cannot be accounted for by either of the two crystal structures.

Adapted from [14].

presence of a sparsely-populated partially-closed apo state, occupying a region of conformational space similar to, but distinct from, that occupied by the ligand-bound closed holo state, may facilitate the transition to the holo structure that is rendered energetically accessible and stabilized by intermolecular interactions between the two domains and the bound ligand. Since the predominant fluctuations in the apo state do not involve the energetically highly disfavored holo conformation, one can view the conformational changes upon sugar binding as a combination of conformational selection afforded by the partially-closed apo state and induced fit reflected in the conformational transition from the partially-closed apo state to the holo state [13].

Recent theoretical work using accelerated molecular dynamics coupled with adaptive biased force and thermodynamic integration free energy methods was able to reproduce the existence of the partially-closed apo state and suggested that sugar binds more tightly to the partially-closed than to the open apo state [26,27]. However,

the relative contributions of sugar binding to the open and partially-closed state will be dependent upon the time scale of the open to partially-closed transition relative to the characteristic diffusion time for the ligand. Theoretical estimates suggest that the time scale for the former (200 ns to 2 μ s) is 10-fold slower than for the latter (>20 ns), such that the higher affinity of sugar for the partially-closed apo state is unlikely to compensate fully for its low (~5%) occupancy [27]. The predominant binding pathway was therefore proposed to involve the initial binding of the sugar to the CTD of the open apo state, followed by a very rapid transition to the partially-closed state, and a subsequent slower final conformational rearrangement to the closed holo state in which both the NTD and CTD interact with the sugar [27]. However, a pathway in which the sugar also binds directly and concurrently to the partially-closed apo state followed by conformational rearrangement to the closed holo state can also occur.

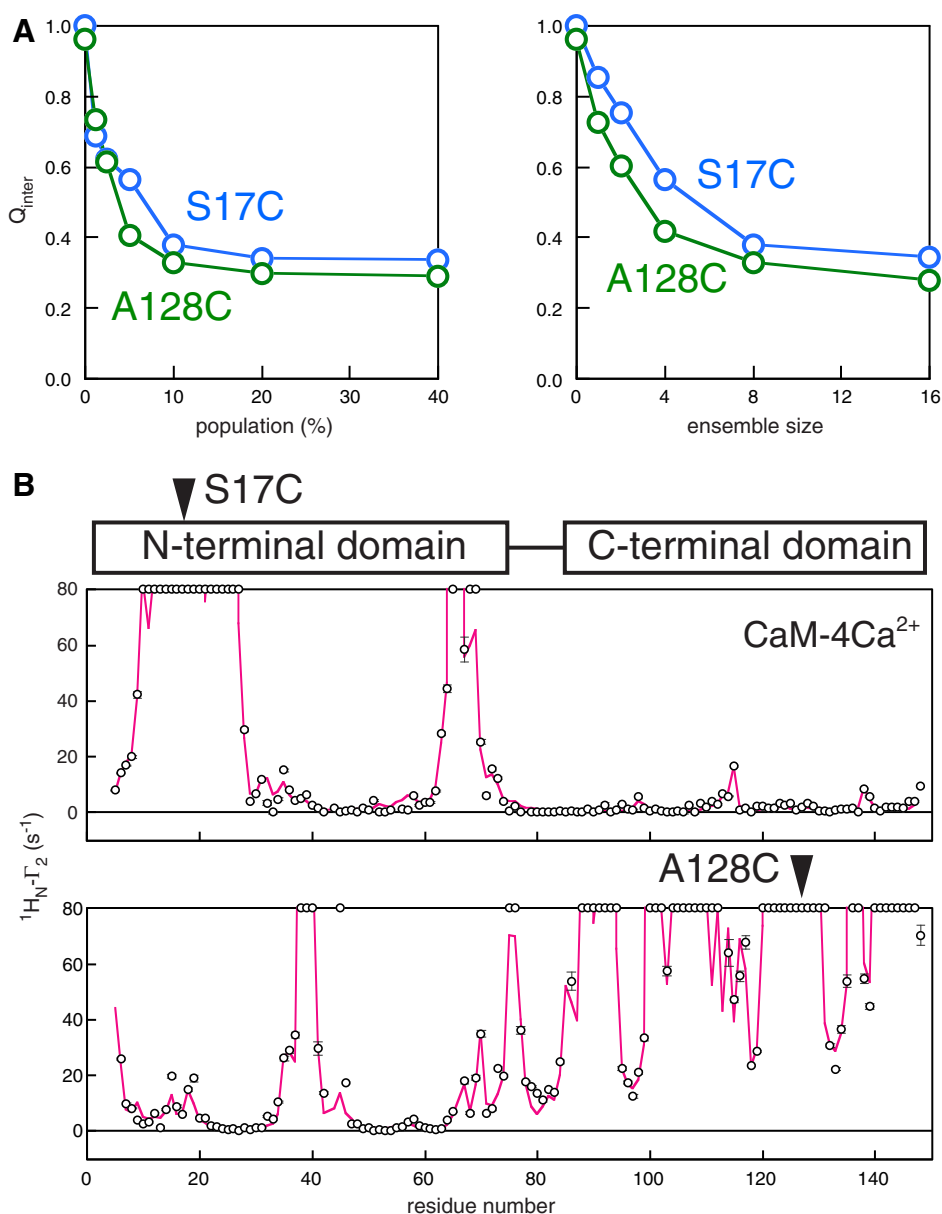


Fig. 7. PRE-driven ensemble simulated annealing refinement for the minor closed states of CaM-4Ca²⁺ characterized by interdomain contacts. (A) Dependence of the interdomain PRE Q-factors for S17C (blue) and A128C (green) as a function of minor-state population (ensemble size $N_e = 8$) (left) and ensemble size (at a minor state population of 10%). (B) Comparison of observed (open circles) and calculated (magenta lines) PRE profiles for S17C (top) and A128C (bottom) for a minor state population of 10% and an ensemble size of $N_e = 8$.

Adapted from [14].

4. Calmodulin

In terms of ligand binding calmodulin (CaM) presents a variation of MBP with a twist. CaM is the primary calcium-sensing protein in eukaryotes and is responsible for amplifying and adapting the effects of Ca^{2+} into specific downstream signals via interactions with hundreds of proteins [28,29]. Like MBP, CaM comprises N- (NTD) and C (CTD)-terminal domains. Unlike MBP, the two domains of CaM are connected by a short flexible linker [30]. In the absence of bound peptide, calcium-bound CaM (CaM-4Ca^{2+}) exhibits a flexible, extended (“open”) conformation with the two domains tumbling semi-independently of one another [30] (Fig. 5). Upon binding peptide CaM-4Ca^{2+} adopts a rigid, compact (“closed”) structure in which the NTD and CTD are clamped round the target peptide (which adopts an α -helical conformation) [31,32] (Fig. 5).

With one exception [33], all crystal structures of free CaM-4Ca^{2+} appear as an extended dumbbell structure with a contiguous helix connecting the two domains separated by a center-to-center distance of ~ 40 Å [34–36] (Fig. 5, top). However, fluorescence [37], and small-angle X-ray and neutron scattering in solution [38] are indicative of an average structure that is somewhat more compact than the extended dumbbell structure. NMR relaxation studies have shown that the central residues (77–81) of the linker are highly mobile (with S^2 order parameters of 0.5–0.6) [30] and that the two domains reorient almost independently of one another on a time scale of ~ 3 ns undergoing restricted diffusion within a cone of semi-angle $\sim 30^\circ$ [39]. Studies based on lanthanide-induced RDCs and pseudo-contact shifts suggest

that an even larger cone of semi-angle 50 – 80° can be sampled [40]. One structure of CaM-4Ca^{2+} has been crystallized in a compact state that loosely resembles the peptide-bound structure [33]. The population of this closed state in solution, however, must be very small as no interdomain NOEs indicative of direct contacts between the NTD and CTD have ever observed [41]. One can therefore conclude that the population of a closed state must be very small in solution.

We made use of PRE measurements to directly probe and visualize compact, sparsely-populated states of CaM-4Ca^{2+} [14]. The results are summarized in Figs. 6 to 8. Significant interdomain PREs are observed with a nitroxide spin label attached to either the NTD (17C) or CTD (A128C) (Fig. 6). While agreement between observed and calculated PREs is excellent for the peptide-bound structure, none of the existing structures can account for the interdomain PRE profiles in the absence of peptide (Fig. 6, bottom panels). Further, while the peaks in the interdomain PRE profiles in the absence of peptide occur at the same locations as in the presence of peptide, the magnitude of the interdomain PREs is very different (Fig. 6, bottom panels), just as was the case with MBP (Fig. 2). One can therefore conclude from a purely qualitative interpretation of the data that there exists an ensemble of closed states in the absence of bound peptide that sample a region of conformational space that is close to but not identical to that of the ligand-bound closed state.

As in the case of MBP, the minor closed state of CaM-4Ca^{2+} can be visualized by PRE-driven conjoined rigid body/torsion angle simulated annealing in which only the linker residues are given torsional degrees of freedom [14]. In contrast to MBP, however, the closed state of CaM-

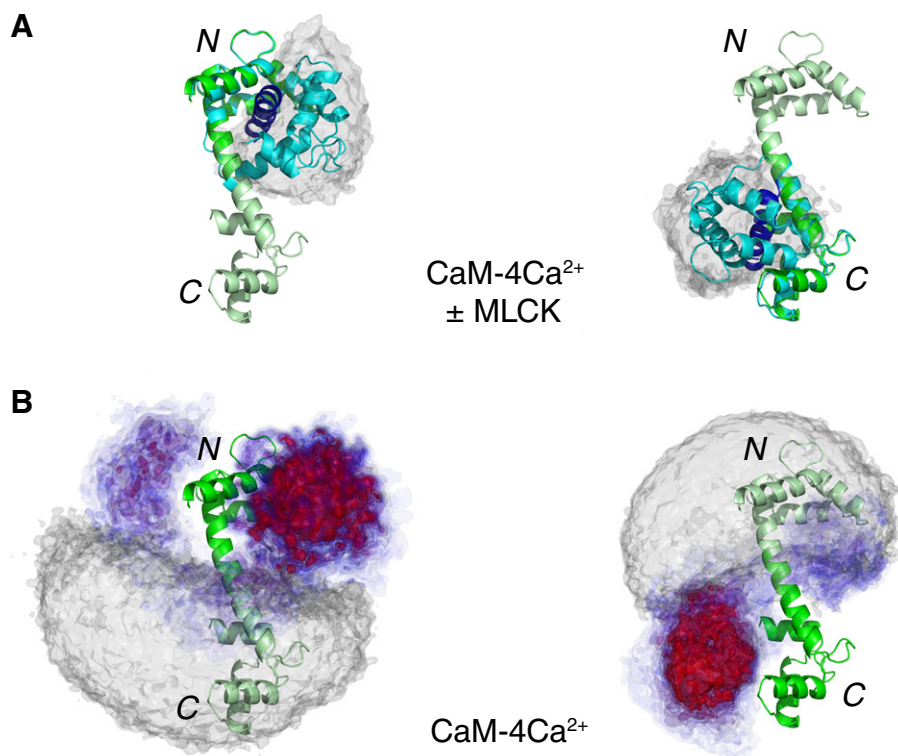


Fig. 8. Visualization of the minor close-state ensemble of CaM-4Ca^{2+} . (A) $\text{CaM-4Ca}^{2+}/\text{MLCK}$ complex [32] (CaM, cyan; MLCK, blue) overlaid on the CaM-4Ca^{2+} dumbbell structure [35] (green), best-fitted to the NTD (left panel) or CTD (right panel). Twenty six additional peptide-bound crystal structures were overlaid in the same manner, and the gray atomic probability map [42] represents their distributions for the CTD (left panel) and NTD (right panel). (B) Atomic probability density maps showing the conformational space sampled by the minor species ensemble with ensemble members best-fitted to either the NTD (left panel) or CTD (right panel). The minor-state atomic probability maps derived from 100 independent simulated annealing calculations (with $N_e = 8$ and a population of 10%) are plotted at multiple contour levels ranging from 0.1 (transparent blue) to 0.5 (opaque red). The gray atomic probability density maps, plotted at a single contour level of 0.1 of maximum, show the conformational space sampled by the major species ensemble (90% occupancy), characterized by no interdomain contacts (i.e. interdomain PRE values restrained to values less than 2 s^{-1}). The extended dumbbell structure is displayed as a ribbon diagram for reference. Approximately half of the minor species ensemble occupies a region of conformational space that is in the vicinity of and overlaps with that of the peptide-bound structure. Adapted from [14].

4Ca^{2+} cannot be represented by a single structure but requires an ensemble of closed and partially-closed states. The results of these calculations are depicted in Figs 7 and 8.

The conformational space compatible with the absence of intermolecular PREs is depicted by the gray atomic probability map [42] which provides a rough guide for the major species (~90%) for which there are no intermolecular contacts (Fig. 8B) (the probability map for the major species generated in this manner is only approximate since it is defined by the absence of intermolecular PREs rather than by any direct experimental measurements). The conformational space occupied by one domain relative to the other occupies a hemisphere with a cone of semi-angle $\sim 90^\circ$ whose distribution and tilt from the crystallographic dumbbell structure is very similar to the ensemble calculated on the basis of pseudo-contact shift, RDC and small-angle X-ray scattering data [43].

The atomic probability maps describing the conformational space sampled by the sparsely-populated (~10%) compact states is plotted in Fig. 8B at multiple contour levels ranging from 0.1 (transparent blue) to 0.5 (opaque red) of maximum [14]. Approximately half of the compact minor species ensemble (i.e. ~5% of the total population) samples a region of conformational space that overlaps with that occupied by CaM-4Ca^{2+} /peptide complexes (Fig. 8A and B).

Thus, the PRE data for CaM-4Ca^{2+} provide direct and unambiguous evidence that the two domains of CaM-4Ca^{2+} come into close contact with one another for a small fraction of the time (~10%) and that these compact states preferentially adopt peptide-bound like configurations about half of the time (~5%) [14] (Fig. 8B). The heterogeneity of this population of closed states coupled with their short lifetimes and low population renders them invisible to conventional NOE measurements.

The PRE data demonstrates unambiguously that CaM-4Ca^{2+} has the ability to form physiologically relevant compact structures that prime it to bind peptide when present. CaM-4Ca^{2+} does not necessarily sample the peptide-bound closed state directly which, in any case, would not be productive since the binding surface would be largely inaccessible to peptide, but rather samples a range of nearby conformations.

The population of the closed and partially-closed states sampled by CaM-4Ca^{2+} is intimately related to the length and rigidity of the linker [44]. Interestingly the linker of CaM is highly conserved and its length invariant. PRE measurements indicate that transient interdomain association is maximal for a linker extended by one residue from the wild-type length and decreases for lengths longer and shorter than that [44]. These results can be quantitatively rationalized using a simplified model of a random coil whose two ends must be a specific distance apart for an interaction to occur [45]. Further, the extent of transient interdomain association as monitored by PRE measurements correlates well with the affinity of CaM-4Ca^{2+} for target peptides which suggests that the transient compact states adopted in the absence of peptide play a direct role in facilitating peptide binding [44].

5. Concluding remarks

MBP and CaM are representative of a very broad class of proteins in which ligand binding results in rigid body interdomain reorientations that effectively trap the ligand and bury it from solvent. In both cases PRE data demonstrate conclusively the existence of short-lived partially-closed, sparsely-populated states in the absence of ligand [13,14] that are invisible to conventional structural and biophysical techniques. The holo conformation, even if significantly populated, cannot bind ligand directly since the ligand-binding site is not accessible (cf. Fig. 4E). However, the existence of sparsely-populated states that are partially closed, occupy a region of conformational space in close proximity to that of the holo state, and are available for ligand binding, may facilitate the transition to the closed-ligand bound complexes. As such both MBP and CaM highlight the

complementarity and interplay of conformational selection and induced fit, with the former characterized by the existence of partially-closed states and the latter by the transition to the final holo state, subsequent to initial ligand binding to either the open or partially-closed apo states. Further, as suggested by accelerated MD simulations [27], the transient ligand-bound partially-closed state can be accessed either by direct binding to the partially-closed apo state or by a rapid conformational transition following ligand binding to the open apo state. Which pathway predominates will depend upon the time scale of the open to partially-closed state transition in the absence of ligand, the characteristic ligand diffusion time, the concentration of protein and ligand, and the relative affinities of the open and partially-closed apo states for the ligand.

The PRE approach for detecting and visualizing sparsely-populated states is applicable to a wide-range of problems pertaining to transient, short-lived conformational transitions in proteins. Transitions involving large rigid body interdomain reorientations are particularly suitable, but any type of transition (e.g. loop rearrangements) can also be studied providing sufficient paramagnetic center–proton distances are available to characterize the conformational states involved. Detection of transient sparsely-populated states by PRE is not only dependent upon rapid exchange between the major and minor species to transfer information from the minor state(s) to the spectroscopically observed major state, but also requires that there exist paramagnetic center–proton distances that are significantly shorter in the minor species than the major one. Transitions involving states where the paramagnetic center–proton distances are longer in the minor species than the major one will be invisible to PRE measurements.

Acknowledgments

G.M.C. thanks members of his laboratory, past and present, and colleagues who have made significant contributions to the development of the PRE to detect sparsely-populated states, in particular, J. Iwahara, C. Tang, C.D. Schwieters, J.-Y. Suh, N. Fawzi, Y. Takayama and N. Anthis. This work was supported by funds from the Intramural Program of the NIH, NIDDK, and the Intramural AIDS Targeted Antiviral Program of the Office of the Director of the NIH (to G.M.C.).

References

- [1] D.E. Koshland, Application of a theory of enzyme specificity to protein synthesis, *Proc. Natl. Acad. Sci. U. S. A.* 44 (1958) 98–104.
- [2] D.E. Koshland Jr., Enzyme flexibility and enzyme action, *J. Cell. Comp. Physiol.* 54 (1959) 245–258.
- [3] J. Monod, J.P. Changeux, F. Jacob, Allosteric proteins and cellular control systems, *J. Mol. Biol.* 6 (1963) 306–329.
- [4] J. Monod, J. Wyman, J.P. Changeux, On the nature of allosteric transitions: a plausible model, *J. Mol. Biol.* 12 (1965) 88–118.
- [5] M.M. Rubin, J.P. Changeux, On the nature of allosteric transitions: implications of non-exclusive ligand binding, *J. Mol. Biol.* 21 (1966) 265–274.
- [6] A.S. Burgen, Conformational changes and drug action, *Fed. Proc.* 40 (1981) 2723–2728.
- [7] D.D. Boehr, R. Nussinov, P.E. Wright, The role of dynamic conformational ensembles in biomolecular recognition, *Nat. Chem. Biol.* 5 (2009) 789–796.
- [8] G.G. Hammes, Y.C. Chang, T.G. Oas, Conformational selection or induced fit: a flux description of reaction mechanism, *Proc. Natl. Acad. Sci. U. S. A.* 106 (2009) 13737–13741.
- [9] P. Csermely, R. Palotai, R. Nussinov, Induced fit, conformational selection and independent dynamic segments: an extended view of binding events, *Trends Biochem. Sci.* 35 (2010) 539–546.
- [10] A.D. Vogt, E. Di Cera, Conformational selection or induced fit? A critical appraisal of the kinetic mechanism, *Biochemistry* 51 (2012) 5894–5902.
- [11] J. Iwahara, G.M. Clore, Detecting transient intermediates in macromolecular binding by paramagnetic NMR, *Nature* 440 (2006) 1227–1230.
- [12] C. Tang, J. Iwahara, G.M. Clore, Visualization of transient encounter complexes in protein–protein association, *Nature* 444 (2006) 383–386.
- [13] C. Tang, C.D. Schwieters, G.M. Clore, Open-to-closed transition in apo maltose-binding protein observed by paramagnetic NMR, *Nature* 449 (2007) 1078–1082.
- [14] N.J. Anthis, M. Doucleff, G.M. Clore, Transient, sparsely populated compact states of apo and calcium-loaded calmodulin probed by paramagnetic relaxation enhancement: interplay of conformational selection and induced fit, *J. Am. Chem. Soc.* 133 (2011) 18966–18974.

- [15] G.M. Clore, J. Iwahara, Theory, practice, and applications of paramagnetic relaxation enhancement for the characterization of transient low-population states of biological macromolecules and their complexes, *Chem. Rev.* 109 (2009) 4108–4139.
- [16] G.M. Clore, A.M. Gronenborn, Structures of larger proteins in solution: three- and four-dimensional heteronuclear NMR spectroscopy, *Science* 252 (1991) 1390–1399.
- [17] J. Iwahara, C. Tang, G.M. Clore, Practical aspects of ^1H transverse paramagnetic relaxation enhancement measurements on macromolecules, *J. Magn. Reson.* 184 (2007) 185–195.
- [18] R. Tam, M.H. Saier Jr., Structural, functional, and evolutionary relationships among extracellular solute-binding receptors of bacteria, *Microbiol. Rev.* 57 (1993) 320–346.
- [19] A.J. Sharff, L.E. Rodseth, J.C. Spurlino, F.A. Quijoch, Crystallographic evidence of a large ligand-induced hinge-twist motion between the two domains of the maltodextrin binding-protein involved in active-transport and chemotaxis, *Biochemistry* 31 (1992) 10657–10663.
- [20] F.A. Quijoch, J.C. Spurlino, L.E. Rodseth, Extensive features of tight oligosaccharide binding revealed in high-resolution structures of the maltodextrin transport chemosensory receptor, *Structure* 5 (1997) 997–1015.
- [21] J. Evenas, V. Tugarinov, N.R. Skrynnikov, N.K. Goto, R. Muhandiram, L.E. Kay, Ligand-induced structural changes to maltodextrin-binding protein as studied by solution NMR spectroscopy, *J. Mol. Biol.* 309 (2001) 961–974.
- [22] C.D. Schwieters, G.M. Clore, Internal coordinates for molecular dynamics and minimization in structure determination and refinement, *J. Magn. Reson.* 152 (2001) 288–302.
- [23] M. Clore, C.D. Schwieters, Theoretical and computational advances in biomolecular NMR spectroscopy, *Curr. Opin. Struct. Biol.* 12 (2002) 146–153.
- [24] J. Iwahara, C.D. Schwieters, G.M. Clore, Ensemble approach for NMR structure refinement against ^1H paramagnetic relaxation enhancement data arising from a flexible paramagnetic group attached to a macromolecule, *J. Am. Chem. Soc.* 126 (2004) 5879–5896.
- [25] O. Millet, R.P. Hudson, L.E. Kay, The energetic cost of domain reorientation in maltose-binding protein as studied by NMR and fluorescence spectroscopy, *Proc. Natl. Acad. Sci. U. S. A.* 100 (2003) 12700–12705.
- [26] D. Bucher, B.J. Grant, P.R. Markwick, J.A. McCammon, Accessing a hidden conformation of the maltose binding protein using accelerated molecular dynamics, *PLoS Comput. Biol.* 7 (2011) e1002034.
- [27] D. Bucher, B.J. Grant, J.A. McCammon, Induced fit or conformational selection? The role of the semi-closed state in the maltose binding protein, *Biochemistry* 50 (2011) 10530–10539.
- [28] M. Zhang, T. Tanaka, M. Ikura, Calcium-induced conformational transition revealed by the solution structure of apo calmodulin, *Nat. Struct. Biol.* 2 (1995) 758–767.
- [29] A.P. Yamniuk, H.J. Vogel, Calmodulin's flexibility allows for promiscuity in its interactions with target proteins and peptides, *Mol. Biotechnol.* 27 (2004) 33–57.
- [30] G. Barbato, M. Ikura, L.E. Kay, R.W. Pastor, A. Bax, Backbone dynamics of calmodulin studied by ^{15}N relaxation using inverse detected two-dimensional NMR spectroscopy: the central helix is flexible, *Biochemistry* 31 (1992) 5269–5278.
- [31] M. Ikura, G.M. Clore, A.M. Gronenborn, G. Zhu, C.B. Klee, A. Bax, Solution structure of a calmodulin-target peptide complex by multidimensional NMR, *Science* 256 (1992) 632–638.
- [32] W.E. Meador, A.R. Means, F.A. Quijoch, Target enzyme recognition by calmodulin — 2.4 Å structure of a calmodulin-peptide complex, *Science* 257 (1992) 1251–1255.
- [33] J.L. Fallon, F.A. Quijoch, A closed compact structure of native Ca^{2+} -calmodulin, *Structure* 11 (2003) 1303–1307.
- [34] Y.S. Babu, J.S. Sack, T.J. Greenhough, C.E. Bugg, A.R. Means, W.J. Cook, Three-dimensional structure of calmodulin, *Nature* 315 (1985) 37–40.
- [35] R. Chattopadhyaya, W.E. Meador, A.R. Means, F.A. Quijoch, Calmodulin structure refined at 1.7 Å resolution, *J. Mol. Biol.* 228 (1992) 1177–1192.
- [36] M.A. Wilson, A.T. Brunger, The 1.0 Å crystal structure of Ca^{2+} -bound calmodulin: an analysis of disorder and implications for functionally relevant plasticity, *J. Mol. Biol.* 301 (2000) 1237–1256.
- [37] B.D. Slaughter, J.R. Unruh, M.W. Allen, R.J. Bieber Urbauer, C.K. Johnson, Conformational substates of calmodulin revealed by single-pair fluorescence resonance energy transfer: influence of solution conditions and oxidative modification, *Biochemistry* 44 (2005) 3694–3707.
- [38] J. Trewthella, The solution structures of calmodulin and its complexes with synthetic peptides based on target enzyme binding domains, *Cell Calcium* 13 (1992) 377–390.
- [39] J.L. Baber, A. Szabo, N. Tjandra, Analysis of slow interdomain motion of macromolecules using NMR relaxation data, *J. Am. Chem. Soc.* 123 (2001) 3953–3959.
- [40] I. Bertini, C. Del Bianco, I. Gelis, N. Katsaros, C. Luchinat, G. Parigi, M. Peana, A. Provenzani, M.A. Zoroddu, Experimentally exploring the conformational space sampled by domain reorientation in calmodulin, *Proc. Natl. Acad. Sci. U. S. A.* 101 (2004) 6841–6846.
- [41] J.J. Chou, S.P. Li, C.B. Klee, A. Bax, Solution structure of Ca^{2+} -calmodulin reveals flexible hand-like properties of its domains, *Nat. Struct. Biol.* 8 (2001) 990–997.
- [42] C.D. Schwieters, G.M. Clore, Reweighted atomic densities to represent ensembles of NMR structures, *J. Biomol. NMR* 23 (2002) 221–225.
- [43] A. Bertini, C. Giachetti, G. Luchinat, M.V. Parigi, R. Petoukhov, E. Pierattelli, D.I. Ravera, Svergun, Conformational space of flexible biological macromolecules from average data, *J. Am. Chem. Soc.* 132 (2010) 13553–13558.
- [44] N.J. Anthis, G.M. Clore, The length of the calmodulin linker determines the extent of transient interdomain association and target affinity, *J. Am. Chem. Soc.* 135 (2013) 9648–9651.
- [45] V.M. Krishnamurthy, V. Semetey, P.J. Bracher, N. Shen, G.M. Whitesides, Dependence of effective molarity on linker length for an intramolecular protein-ligand system, *J. Am. Chem. Soc.* 129 (2007) 1312–1320.